CrossMark

ORIGINAL PAPER

Bound and free water distribution in wood during water uptake and drying as measured by 1D magnetic resonance imaging

Özlem Gezici-Koç · Sebastiaan J. F. Erich · Hendrik P. Huinink · Leendert G. J. van der Ven · Olaf C. G. Adan

Abstract Knowledge on moisture transport in wood is important for understanding its utilization, durability and product quality. Moisture transport processes in wood can be studied by Nuclear Magnetic Resonance (NMR) imaging. By combining NMR imaging with relaxometry, the state of water within wood can be identified, i.e. water bound to the cell wall, and free water in the cell lumen/vessel. This paper presents how the transport of water can be monitored and quantified in terms of bound and free water during water uptake and drying. Three types of wood from softwood to hardwood were selected covering a range of low to high density wood; pine sapwood and oak and teak. A calibration is performed to determine the different water states in each different wood type and to convert the NMR signal into moisture content. For all wood types, water transport appeared to be internally limited during both uptake and drying. In case of water uptake, free water was observed only after the cell walls were saturated with bound water. In case of drying, the loss of bound water starts only after vanishing of free water, irrespective of the position. Obviously, there is always a local thermodynamic equilibrium of bound and free water for both uptake and drying. Finally, we determined the effective diffusion coefficient (D_{eff}). Experimentally determined diffusion constants were compared with those derived by the diffusion models for conceptual understanding of transport mechanism. We found that diffusion in the cell wall fibers plays a critical role in the transport process.

Keywords Wood · Moisture content · NMR imaging · Water uptake · Drying · Diffusivity

Abbreviations

NMR	Nuclear Magnetic Resonance
FSP	Fiber Saturation Point
RF	Radio Frequency
CPMG	Carr-Purcell-Meiboom-Gill
HSE	Hahn Spin Echo
MC	Moisture Content
EMC	Equilibrium Moisture Content
RH	Relative Humidity
DVS	Dynamic Vapor Sorption
SI	Signal Intensity

List of symbols

f	Resonance frequency
$\vec{B}$	Applied magnetic field

Ö. Gezici-Koç · S. J. F. Erich (✉) ·
H. P. Huinink · L. G. J. van der Ven · O. C. G. Adan
Department of Applied Physics, Eindhoven University of Technology, P.O. Box 513, 5600 MB Eindhoven, The Netherlands
e-mail: s.j.f.erich@tue.nl

S. J. F. Erich · O. C. G. Adan
TNO, The Netherlands Organization for Applied Scientific Research, P.O. Box 49, 2600 AA Delft, The Netherlands

$\overrightarrow{B_0}$ Main magnetic field in the z-direction

γ Gyromagnetic ratio ($\gamma = 42.58$ MHz/T for hydrogen nuclei)

$\overrightarrow{G_z}$ Linear magnetic field gradient in the z-direction

T_2 Relaxation time that describes the decay of the NMR signal

α Flip angle

τ Pulse time

t_e Interecho time

n Number of echoes

I NMR signal

Δx Theoretical spatial resolution

n_{avg} Number of signal averages

t_{RT} Repetition time between two subsequent pulses

D_{eff} Effective diffusion coefficient

Z Position

t time

t_{ww} Recording window

θ Moisture content

θ_∞ Initial moisture content

θ_0 Boundary moisture content

D_v Water vapor diffusion coefficient

D_b Bound-water diffusion coefficient

c_v Molar density of water vapor

c_b Molar density of bound water

τ Tortuosity of wood for vapor

L_b The length of the path for bound water

L_v The length of the path for water vapor

J Flux

Introduction

Wood is a hygroscopic and porous material in which the distribution and interactions of water play a crucial role in wood processing and durability. In many situations and applications, wood is undergoing fluctuations in moisture content due to periodic water absorption and desorption. Understanding the water absorption and desorption characteristics of wood is of practical importance, since the mechanical properties or the dimensional stability of wood are influenced by the moisture content. Moreover, a high moisture content may result in durability loss due to fungal growth and/or delamination of an applied protective layer.

In wood, water can be present in two states. First, the water can reside in cell walls, which is called bound water. Second, water may exist in liquid pockets located in the cell lumen and other void spaces, called free water. Generally, one can observe a transition from a regime where only bound water is present towards a regime where free and bound water are present together. The point where this transition occurs is called the Fiber Saturation Point (FSP) (Stamm 1971). Understanding the transport properties requires understanding the changes in bound and free water (Topgaard and Söderman 2002). Although many studies have been performed to understand water transport properties, it is not easy to identify the state of water within wood, and especially to determine each state during uptake or drying by experimental techniques, such as weighing (Wiberg et al. 2000) or X-ray computer tomography (CT) (Sandberg and Salin 2010) or neutron radiography (Sedighi-Gilani et al. 2012).

One of the methods to study water in wood is Nuclear Magnetic Resonance (NMR) Imaging. It is a non-invasive method that provides temporally and spatially resolved moisture profiles (Bucur 2003). The intensity of the NMR signal is proportional to the number of hydrogen nuclei in the sample, i.e. the water content. NMR Imaging has been proven to be an excellent tool to determine the distribution and the concentration of water in wood during drying (Quick et al. 2007; Stenström et al. 2014; Dvinskikh et al. 2011a, b), and during uptake (Robertson and Packer 1999; Van Meel et al. 2011; Donkers et al. 2013). In situ determination of local moisture content has been achieved by portable NMR devices (Casieri et al. 2004; Dvinskikh et al. 2011b). Another important advantage of NMR over other methods is its ability to distinguish between bound and free water by relaxation analysis (T_2), i.e. the decay of the NMR signal (Riggin et al. 1979; Menon et al. 1987; Araujo et al. 1992; Telkki et al. 2013). For detailed information, please see section "Relaxation analysis of water in wood".

To understand the transport properties, moisture profile determination and water state characterization during water uptake and drying should be carried out. In previous studies with NMR, such determination of moisture profiles and characterization of water states during drying was achieved for yellow poplar (Zhang et al. 2013), Douglas fir (Menon et al. 1987), red cedar (Menon et al. 1987; Quick et al. 2007), Norway spruce (Thygesen and Elder 2009) and Scots pine (Hameury

et al. 2006; Rosenkilde and Glover 2002). These studies provide spatially resolved one dimensional moisture profiles, but no spatially resolved relaxation analysis. The role of the porosity on water transport was studied by Kekkonen et al. (2014). They investigated absorption of water in thermally modified wood by applying various NMR methods. Their results show that thermal modification partially blocks the access of water to cell walls. The noticeable decrease in free water for the samples modified above 200 °C indicate that large amount of pits connecting wood cells are closed due to high modification temperature.

In this work, we aim to visualize and quantify bound and free water distribution for pine sapwood, oak and teak during water uptake and drying by using NMR imaging and relaxometry. More specifically, five subsequent steps are taken to answer to this objective. The first step is to discriminate between bound and free water in the measured signal, i.e. to calibrate the signal. The second step is to convert the NMR signal into moisture content. In the third step we monitor and quantify the changes in bound and free water, and the order of filling/emptying of each state during uptake and drying, whereas in the fourth step the effective diffusion coefficient, D_{eff}, is determined. Finally, in the fifth step these experimental D_{eff} values are compared with those derived by two diffusion models.

Materials and methods

Wood types

The selected wood types and their characteristic properties are given in Table 1.

Wood has a complex heterogeneous microporous structure. Optical microscope images of pine sapwood, oak and teak are given in Fig. 1, in which the heterogeneity in the samples is visible The microscopic cellular structure of wood, including annual growth rings and rays, presents the characteristic patterns in different wood types. For all studied wood types, annual growth rings are visible with earlywood (spring) and latewood (summer) rings. Rays are the radial cells, running perpendicular to growth rings, which provide radial transport. As shown in the inset sketch, the inner cavity of a wood cell is called the lumen, and the surrounding structural layer is the cell wall, which consists mainly of cellulose, playing an important role in the wood-water relationship. Wood cells are equipped with pits that serve as passages of transport between neighbouring cells.

Wood is classified as either a hardwood or softwood; they differ in the physical structure. Hardwoods have more complicated anatomical features and greater structural variation compared to softwoods, which results a greater range in permeability and capillary behaviour (Siau 1984). Hardwoods have a higher density than most softwoods. In softwoods, such as pine, the water transport throughout the wood is achieved by elongated cells, called tracheids, which are running lengthwise with the trunk. The diameter of tracheids can vary based on being earlywood or latewood tracheid. In pine sapwood, earlywood cells have thinner cell wall and larger lumen, while latewood cells have thicker cell wall and smaller lumen. The primary distinguishing feature between softwoods and hardwoods is that hardwoods, such as oak and teak, have vessels, i.e. pores, that transport water throughout the wood. In some species, such as oak, the earlywood has larger pores compared to the latewood, in which they are characteristically known as "ring-porous" wood. In some other species, such as teak, the pore size gradually decreases from the earlywood to the latewood, but the pores do not form clear rows as observed in ring-porous woods. They are known as "semi-ring porous" wood.

Table 1 Selected wood types and their general characteristics

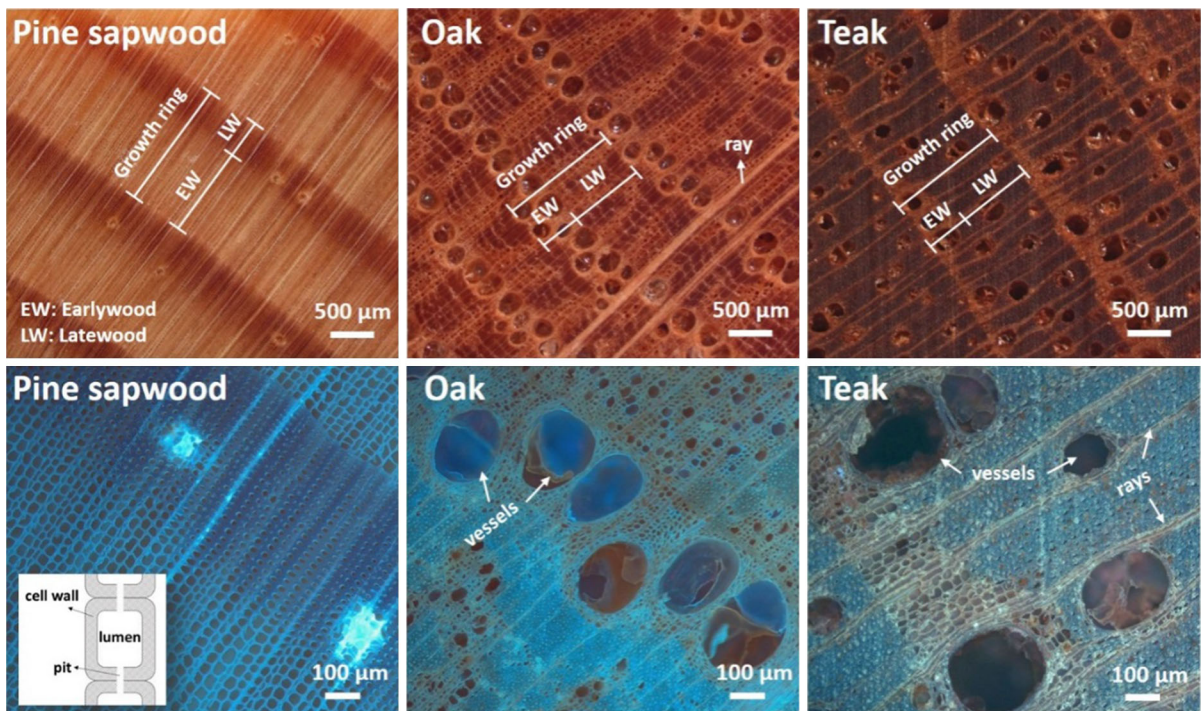| Wood type	Softwood/hardwood	Density (kg/dm³)	Structure
Pine sapwood (*Pinus sylvestris*)	Softwood	∼0.54	No vessels
Oak (*Quercus petraea*)	Hardwood	∼0.64	Ring porous
Teak (*Tectona grandis*)	Hardwood	∼0.64	Semi-ring porous

Fig. 1 Optical microscope images of cross-sections of pine sapwood, oak and teak. The *above* "overview" images are with incident halogen light, the *below* "detailed" images are with UV light. The *inset* presents a simple sketch of a wood cell

Next to structural differences between the studied wood types, there are differences in the cut directions. Figure 2 is a schematic diagram of wood log showing different cut directions is presented.

In this study, the pine panels have a radial cut in which the rays are almost parallel and the growth rings, i.e. longitudinal tracheids, are almost

Fig. 2 The schematic diagram of wood log showing different cut directions

perpendicular to the surface. Teak and oak have a tangential cut where the growth rings and rays are oriented diagonally (about 45° angle) to the surface, but perpendicular to each other.

NMR imaging and relaxometry

Principles

The NMR principle is based on exciting the magnetic nuclei, in our case hydrogen nuclei, placed in a magnetic field by a radio frequency (RF) pulse and detecting the induction in an RF coil. The resonance frequency, f, of the magnetic nuclei depends on the magnitude of the applied magnetic field, $\vec{B}$, according to $f = \gamma|\vec{B}|$, wherein γ is the gyromagnetic ratio ($\gamma = 42.58$ MHz/T for hydrogen nuclei). In order to obtain spatial information, the resonance frequency is varied with position according to $f = \gamma(B_0 + zG_z)$, wherein G_z represents the linear magnetic field gradient in the z-direction, and $\overrightarrow{B_0}$ is the main magnetic field in the z-direction. The NMR signal
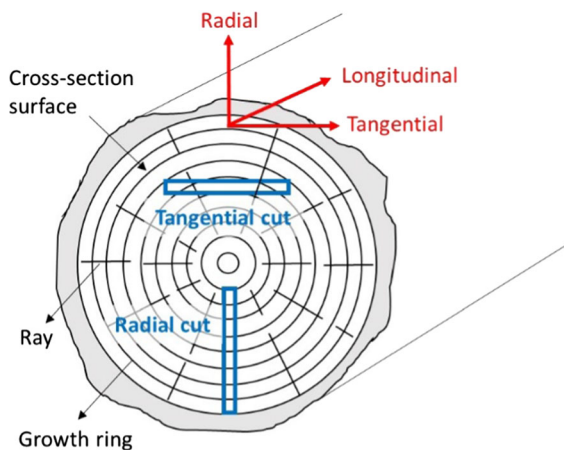
gives information on the mobility of the magnetic nuclei, in our case hydrogen nuclei, next to giving the density (concentration) of these nuclei. As the water molecules (i.e. the hydrogen containing molecules) inside the pores are excited by an NMR pulse, diffusion causes random collisions between the water molecules and the pore walls, which in turn causes relaxation, T_2, which describes the decay of the NMR signal. T_2 is related to local mobility, i.e. T_2 is longer when freely moving water molecules are in bulk water or shorter when their mobility is restricted by a small volume.

Settings

A main magnetic field of 0.75 T was used with a constant gradient of 418 mT/m in the z-direction, i.e. parallel to $\overrightarrow{B_0}$. In the experiments, the center of the sample was aligned at the isocenter of the magnet. Slice selection was achieved by turning on linear magnetic field gradient, G_z, while applying an excitation pulse that allows rotating the spins, which are located in a slice through the sample. The sample was kept at a fixed position and multiple slices covering the whole sample were obtained by varying the center frequency, as illustrated in Fig. 3.

Hahn Spin Echo (HSE) sequence (Hahn 1950), $\alpha_x° - \tau - 2\alpha_y° - \tau - echo - \tau$, was used to obtain the hydrogen density profiles, where α is the flip angle and nominally equals to 90° with a pulse time of 25 μs. A Carr-Purcell-Meiboom-Gill (CPMG) sequence (Carr and Purcell 1954), $\alpha_x° - \tau - [2\alpha_y° - \tau -$

echo $- \tau]_n$, was used to measure the relaxation time at several points through the whole sample. n is the number of echoes. The interecho time ($t_e = 2\tau$) used in the experiments equals 200 μs, while the recording window (t_{ww}) to measure the echo has a duration of 120 μs. The resulting NMR signal shows an exponential decay, as described by:

$$I(\tau) = \sum_{i=1}^{m} I_i exp\left(-n \times 2\tau / T_2^i\right), \qquad (1)$$

where $I(\tau)$ is the observed NMR signal at a time, I_i is the signal from each exponential component, and m is the number of components. The signal intensity of each exponential term is proportional to the pore volume. Therefore, the signal intensity of each term versus T_2 values produces a continuous spectrum of T_2 values, i.e. a map of the volume occupied by each pore size or the pore size distribution.

Note that the height and width of the T_2 peaks are dependent on the quality of the fit. The peak maximum value is taken for the relaxation time determination and the area under the peak is proportional to the volume occupied by each component (Gezici-Koç et al. 2016).

The settings are summarized in Table 2. Δx is the theoretical spatial resolution, n_{avg} is the number of signal averages, and t_{RT} is the repetition time between two subsequent pulses.

The measured signal profiles are divided by the signal profile of a homogeneous reference sample (same volume) allowing the local hydrogen density to be determined. As a reference sample, an aqueous 0.01 M $CuSO_4$ solution was used.
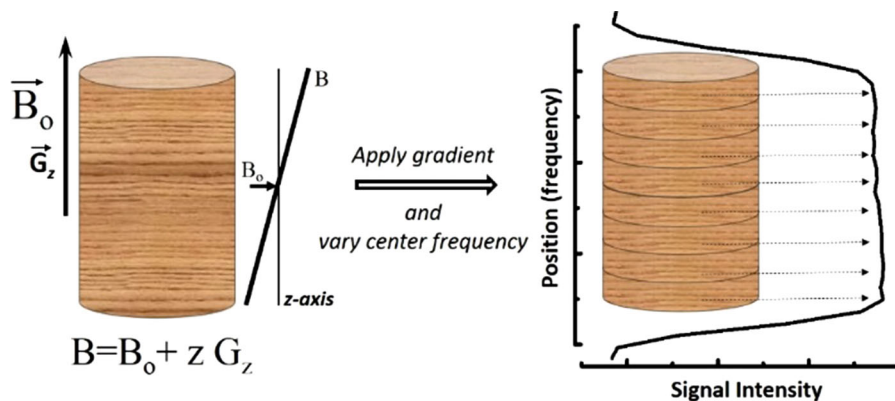
Fig. 3 Slice selection by NMR

Table 2 The measurement settings of HSE and CPMG pulse sequences used during water uptake and drying of all selected wood types

	t_e (µs)	t_{ww} (µs)	$t_{90°}$ (µs)	G_z (mT/m)	Δx (mm)	n	n_{avg}	t_{RT} (s)
HSE	200	120	25	418	0.46	–	4	8
CPMG	200	120	25	418	0.46	1024 (water uptake) 2048 (drying)	32	8

Relaxation analysis of water in wood

Several researchers performed relaxation analysis to distinguish water states in wood, especially softwood species (Menon et al. 1987; Araujo et al. 1992, 1993) as it has a simpler anatomical and more homogeneous structure. In softwood, three relaxation times are observed as related to three different environments for the hydrogen nuclei (Menon et al. 1987; Araujo et al. 1992, 1993), i.e. the cellulose of solid wood, water in the lumen and water in the cell wall. Figure 4 shows a schematic presentation of different states of water present in wood.

Cellulose is the main constituent of the cell walls of wood fibres and contributes to the water adsorption of wood through its numerous hydroxyl groups (Siau 1984; Bulian and Graystone 2009).

As in the case **I**, when the moisture content (MC) is far below the FSP, the cell wall water is tightly bound to the hydroxyl groups of cellulose by hydrogen bonds along the chains of the amorphous or paracrystalline regions via reversible processes (Siau 1984). Note that the water does not penetrate into the crystalline regions of cellulose (Skaar 1988). It results in a relatively short relaxation time, called bound water. When the MC increases towards the FSP, as in case **II**,
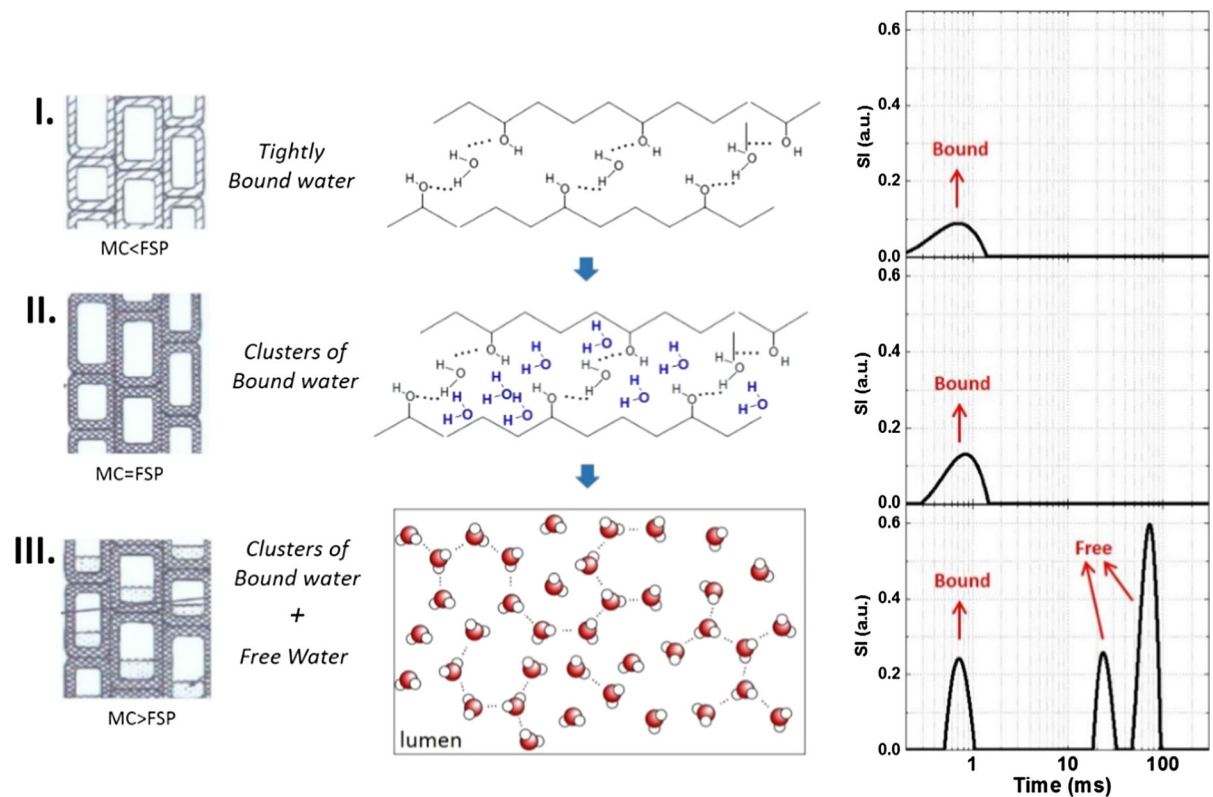

Fig. 4 The schematic presentation of different states of water present in the cell wall and the lumen, the interactions (hydrogen bonds) between water and the hydroxyl groups of cellulose, and the relaxation time distributions, when **a** MC < FSP, **b** MC = FSP, and **c** MC > FSP

more water molecules with an increased mobility are present in the cell wall, resulting in a small increase in the short relaxation time. In fact, one can consider them as clusters of water that are still bound. It is hard to differentiate these two cases (**I** and **II**) by looking at T_2 values, since there may not be a significant difference. On the other hand, a signal increase is observed for case **II** due to an increase in hydrogen nuclei. When the MC increases above the FSP, as in case **III**, water will be present within the lumen having a longer relaxation time, called free water. Different T_2 values in the range of free water result from the presence of different sized lumen or other void spaces. For example, earlywood cells have wider lumen, so longer T_2, compared to latewood cells (Menon et al. 1987; Kekkonen et al. 2014). The wood cellulose has very short T_2 around tens of microseconds, which is too short to be observed in the used NMR set-up. The bound water in the cell wall has a T_2 typically ranging from hundreds of microseconds to several milliseconds, whereas the free water in the lumen has a T_2 typically ranging from ten to hundreds of milliseconds. Additionally, later studies showed an extra slow relaxing component in hardwood due the presence of vessel elements (Almeida et al. 2007; Passarini et al. 2014). The free water in vessels may have higher T_2 values compared to the water in lumen.

Sample preparation for calibrating the NMR signal

To convert the NMR signal to moisture content, calibration was performed for all three wood types. For each type of wood, twelve samples were prepared by cutting small cylinders with a diameter of 20 mm and height of 10 mm. They were initially at room condition having an ambient relative humidity (RH) of about 40%. Then, they were equilibrated at 12, 22, 33, 43, 53, 65, 75, 85, 93, 97 and 100% RH above saturated salt solutions at room temperature (~ 22 °C). One sample from each type of wood was immersed in distilled water to achieve a fully saturated state. Equilibration took at least four weeks and was checked by monitoring the sample weight. The equilibrium moisture content (EMC) is set when the wood reaches a stable moisture content at a certain RH and temperature. After gravimetric determination of EMC of each sample and performing NMR measurements, they are oven dried at 105 ± 2°C for 2 days. The MC is determined gravimetrically and expressed as a percentage, from the ratio of the mass of water divided by the oven dried mass of wood samples. The average of oven dried weight of twelve samples was found as 1.7 ± 0.04 g for pine sapwood, 2.0 ± 0.04 g for oak and 2.0 ± 0.02 g for teak.

Samples and sample holders for water uptake and drying

20 mm diameter cylindrical samples were drilled from 10 mm thick wood panels (radial cut for pine sapwood, and tangential cut for oak and teak). For water uptake and drying measurements, the samples were initially at room condition having an ambient relative humidity (RH) of about 40%. Prior to the water uptake measurements, all samples were equilibrated at 33% RH for at least 4 weeks. Teflon sample holders were used to prevent interference with ^{1}H NMR signal. The sides of the samples were sealed with Teflon grease and Teflon tape, so the water can only enter the wood from the top side. Distilled water was put on top of wood samples.

Prior to the drying measurements, all samples were saturated until their maximum MC was reached. This was achieved by immersing the specimens in distilled water for at least one month. For saturation, the specimens were exposed to water from all sides, and full saturation was checked before the drying experiments were carried out. Teflon sample holders for drying measurements are illustrated in Fig. 5.

They were designed to seal the sides of the sample, so the water can only leave the wood from the top side. The sample holder has two different diameters inside
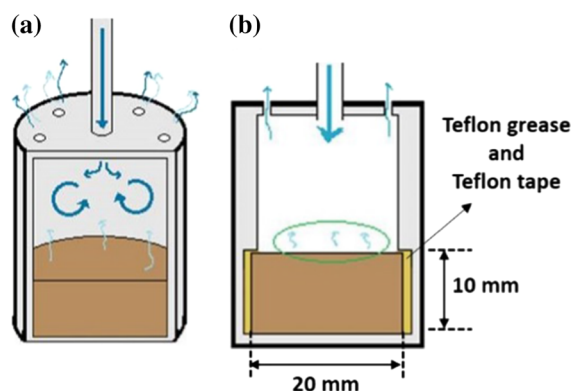

Fig. 5 a An illustration of the sample holder for drying measurements, showing the air flow inside, **b** and the inner structure of the sample holder
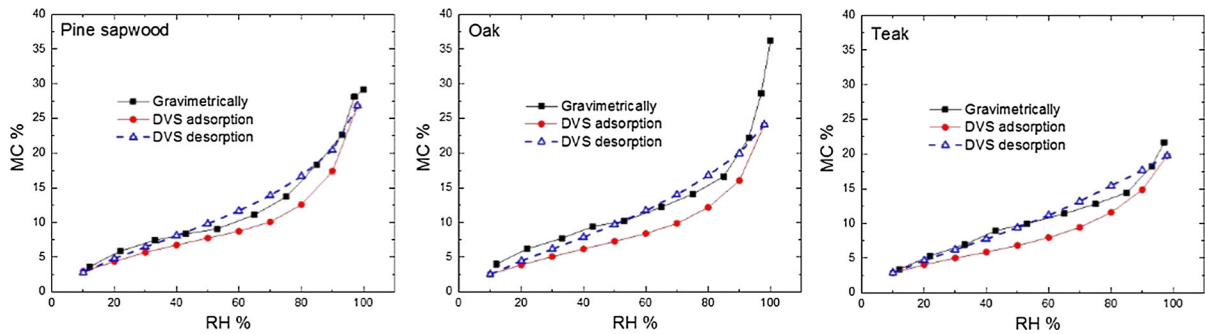
Fig. 6 Sorption isotherms for pine sapwood, oak and teak, determined gravimetrically at 22 °C and measured by Dynamic Vapor Sorption (DVS) at 25 °C

(Fig. 5b). The lower part has a diameter ensuring that the sample is tightly fit. The upper part has a smaller diameter preventing the sample to be moved, and simultaneously prevents water escaping from the sides. To ensure closure of the sides, the sides of the wood samples were covered with Teflon grease and Teflon tape before placing in the holder. Furthermore, dry air was blown from the top of the sample holder. The air flow was set at 3 L/min with an RH about 0–5% at room temperature (~ 22 °C).

Dynamic Vapor Sorption (DVS)

The equilibrium moisture sorption of all samples was analysed using a Dynamic Vapor Sorption (DVS) instrument (Q5000 SA from TA Instruments). The measurements were performed at a constant temperature of 25 °C with an initial sample weight of 2.0–4.0 mg. Weight changes were determined with a thermobalance (weight accuracy of 0.1% and signal resolution of 0.01 μg). Samples were initially dried for 10 h at RH of 10%. The RH was then increased from 10 to 98% (in 10% steps from 10 to 90%, and one 8% step from 90 to 98%), and subsequently decreased in similar steps till 0%. For all RH steps, the instrument was run in a dm/dt mode (mass variation over time variation) to detect when equilibrium was reached.

Results and discussion

Equilibrium water sorption and signal calibration

For a profound analysis of water transport in wood, a full understanding of water binding to the wood is

required. This enables calibration of the NMR signal, as to relate it to the moisture content in pine sapwood, oak and teak.

Sorption isotherms

In Fig. 6, sorption isotherms of pine sapwood, oak, and teak are given quantifying the amount of water in wood at different humidity conditions. Besides gravimetrically determined sorption isotherms, the results of Dynamic Vapor Sorption (DVS) are included. Note that gravimetric determination uses different samples for each RH at 22 °C, whereas DVS concerns one and the unique sample at 25 °C. Although the equilibrium moisture content (EMC) at a certain RH varies for different wood types, the sigmoidal shape of the sorption isotherm is similar for all wood types. The MC increases almost linearly at lower RH region (below 60%), while the MC increases rapidly with humidities above 60% RH. The inflection point is the result of the transition of water in a bound state to the formation of clusters of bound water (see Fig. 4). This transition occurs between 60 and 80% RH for the wood species studied.

For pine sapwood, oak and teak, the gravimetrically determined sorption isotherms are similar to the DVS desorption isotherms. However, the gravimetrically determined sorption isotherm is neither desorption nor adsorption, because the samples were initially at about 40% RH. There is difference between the adsorption and desorption isotherms as measured with DVS, which shows hysteresis for all wood types. The wood hysteresis is not taken into account throughout this study.

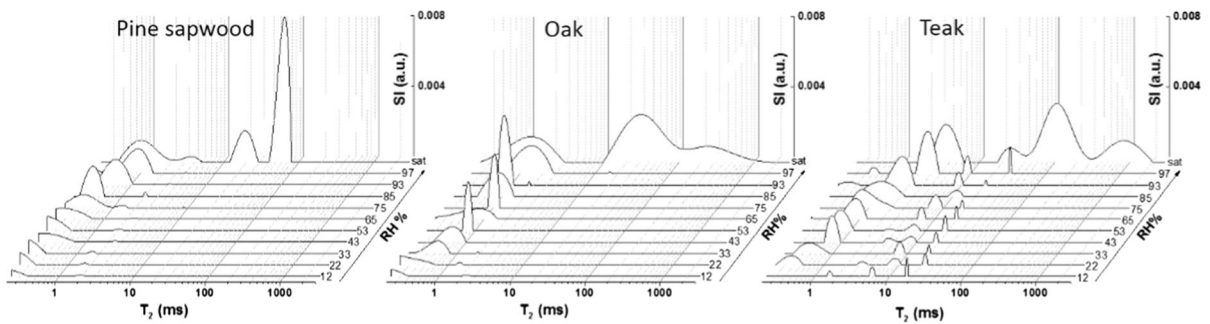The FSP is found to be around a MC of 29% for pine sapwood, 30% for oak and 22% for teak.

Fig. 7 Relaxation time (T_2) distributions of the samples equilibrated at different humidity conditions and fully water saturated sample

Identifying bound and free water at different humidity conditions

Knowing the sorbed amounts, the question is now in which state water molecules are in wood. Therefore, a relaxation analysis is performed at different humidity conditions, see Fig. 7. The figure shows the T_2 distribution plot for the studied wood types at various humidity conditions ranging from 12% to 100% RH and fully water saturated condition.

Pine sapwood

A relaxation time above 10 ms is observed only in the fully saturated sample. At RH below 100%, only short relaxation time is visible, which decreases from 1 ms to the values below 0.2 ms with decreasing RH. A long T_2 observed in the fully saturated sample corresponds to free water in the lumen or in other void spaces. It shows two well-separated relaxation times around 20 and 60 ms due to possible differences in the lumen size. The short $T_2 \leq 1$ ms corresponds to bound water in the cell wall. The decrease in T_2 of bound water with decreasing RH is due to the decrease in the mobility. The water in the bound state below 75% RH has very restricted mobility because of hydrogen bonding with the cellulose of the cell wall. Consequently, it has a very short relaxation time, which is shorter than the echo time used for CPMG measurement, i.e. 200 μs. Since some of the spins corresponding to tightly bound water already relaxed before they were measured, it results in partly detecting the bound water, which is observable in the T_2 distribution plot.

Oak

Compared to pine sapwood, the main difference is that the long relaxation time observed for the fully saturated sample has a very broad distribution ranging from 10 to 300 ms. The broad distribution reflects the polydispersity of the pore sizes. The short T_2 corresponding the bound state is around 1 ms for fully saturated sample, which decreases to lower values around 0.5 ms with decreasing RH till 33%. At 12 and 22% RH, T_2 is even shorter, being below 0.2 ms.

Teak

Comparing the relaxation times corresponding to bound and free water in pine sapwood and oak, there are additional peaks observed for teak. The relaxation time distribution ranging from 30 to 600 ms corresponds to the water in the free state, which is only available in the fully saturated sample. The relaxation time corresponding to bound water is around 3 ms in fully water saturated condition, around 2 ms for high RH (97%), and a shift towards lower values (around 0.5 ms) at relatively dry conditions. The additional peaks are observed between 4 and 30 ms, which seems similar at all RH. We separate the total signal intensity (SI) into the sections of the bound water (below 4 ms) and the additional peaks (between 4 and 30 ms) based on the relaxation analysis in Fig. 7, by summing up the signal intensities in the relative sections. In Fig. 8, the corresponding signal intensities of these two sections are shown versus RH. The gravimetrically determined sorption isotherm is also included in the graph.
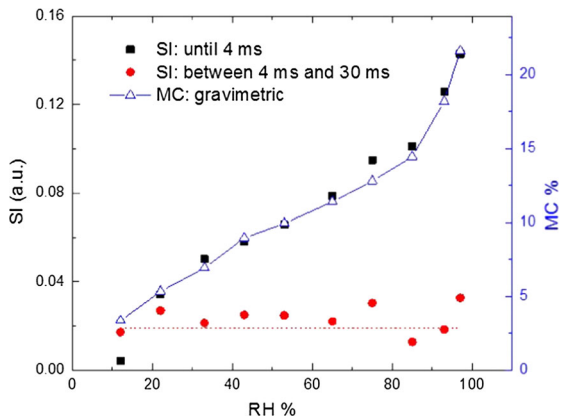
Fig. 8 NMR signal intensities of the section below 4 ms and the section between 4 and 30 ms in the relaxation time distributions of teak at different humidity conditions, and the gravimetrically determined sorption isotherm
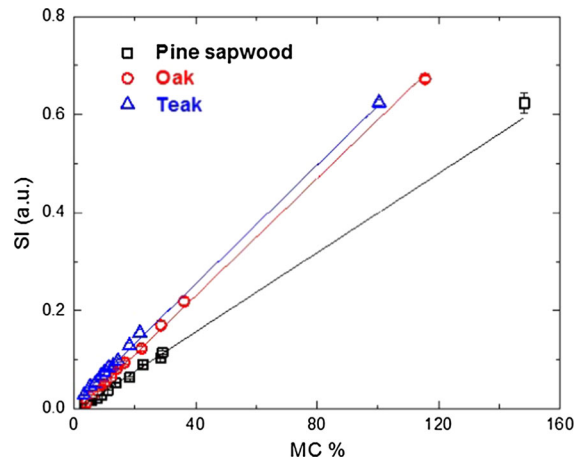

Fig. 9 The signal intensity of the first echo of CPMG versus moisture content (mass percent) for pine sapwood, oak and teak. The *solid lines* are the linear fits

The shape of the measured signal versus RH curve for the section below 4 ms is in agreement with the sorption isotherm. At very low RH ($\sim 10\%$), NMR underestimates the amount of bound water as the T_2 is shorter than the echo time resulting in signal loss. For the section between 4 and 30 ms, the measured signal seems to be around 0.02, irrespective of the RH. This suggests the presence of a component in teak which is not influenced by the water content. It can be low-molecular-weight organic compounds known as extractives (Siau 1984; Peemoeller et al. 2013; Labbé et al. 2002).

Calibrating the NMR signal

The signal intensity (SI) of the first echo of CPMG sequence was calibrated to obtain the total wood moisture content, as shown in Fig. 9.

Based on the average SI versus the MC of each of the equilibrated samples in the range of 12–100% RH and the fully water saturated sample, there is a linear relationship between the corresponding SI and the moisture content for pine sapwood ($R^2 = 0.9770$), oak ($R^2 = 0.9977$) and teak ($R^2 = 0.9947$). The linear regression equations are found as $y = 0.00404x - 0.00451$ for pine sapwood, $y = 0.00598x - 0.00881$ for oak, and $y = 0.00606x + 0.01211$ for teak, where y is the SI and x is the MC expressed as percentage. The small offset found ($<1\%$) in the equations for pine and oak tells us that a minimum moisture content should be present in order to obtain any signal of

water. In case of teak, the contribution from an organic component for teak leads to a small positive offset.

The state of water in wood during water uptake and drying

NMR measurements with temporal and spatial resolution were performed during water uptake and drying of pine sapwood, oak and teak, to understand the moisture transport mechanisms in different wood types from softwood to hardwood. In this section, we focus on the state of water.

Water uptake

Moisture content profiles of pine sapwood during water uptake are given in Fig. 10a. The surface in contact with the liquid water is located at position $x = 0$. The FSP is indicated by horizontal dashed line. The profile prior to water uptake is flat and corresponds for a MC of about 6%, which was equilibrated at 33% RH. During the early phase of the uptake (first 2 days), a front develops indicating that the transport is internally limited. This front occurs until it reaches the bottom, where the MC remains below the FSP. Between 7 and 36 days, there is very little increase in the MC, which still stays around the FSP. After 114 days, the MC significantly exceeds the FSP.

Besides the MC profiles, relaxation analysis is used to identify and quantify the state of water during water uptake. The relaxation analysis is performed at three
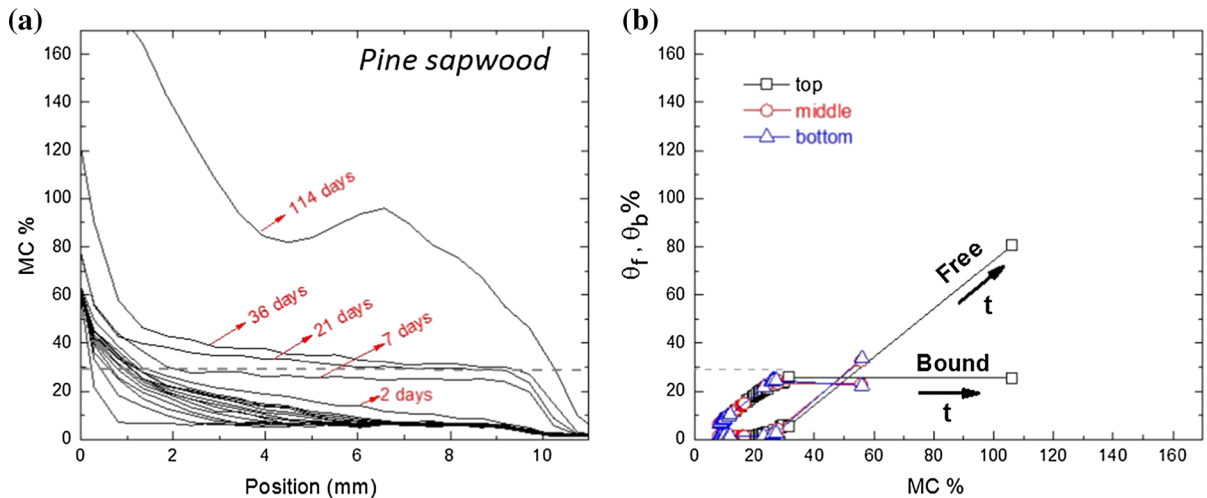
Fig. 10 a The MC profiles of pine sapwood during water uptake for 114 days. The profiles are given every 2 h for the first day and at the indicated times. **b** Moisture fraction of free water,

θ_f, and bound water, θ_b, versus total MC at 3 positions: around 2 mm (*top*), 5 mm (*middle*) and 8 mm (b*ottom*) below the surface

different points, around 2 mm (top), 5 mm (middle) and 8 mm (bottom) below the surface, where it relates to a region of 0.5 mm width at each position. The plot of moisture fractions versus total MC at these three positions is given Fig. 10b. It shows that there is only bound water at initial stages. First the cell walls are filled with bound water, irrespectively of the position. Only after the saturation of the cell walls, free water is observed.

Moisture content profiles of oak and teak during water uptake are given in Fig. 11a and c. Similar to pine sapwood, a front immediately develops indicating that the transport is internally limited for both wood types.

The plots of moisture fractions versus total MC at three different positions for both oak and teak are shown in Fig. 11b and d. At all positions, the bound water is first filled, and then free water is only observed after all the cell walls are saturated. The absence of free water before the cell wall saturation reveals a closed-pore system in all studied wood types. Since the fractions of bound and free water are dependent on the MC, intrinsically a thermodynamic equilibrium is set. Additionally for teak, the moisture fraction of bound water at full saturation of cell walls is around 15%, which is smaller than previously found FSP, 22%. It may result from the difference in the structure of this individual specimen, which differs from the average.

Drying

Moisture content profiles of pine sapwood during drying are given in Fig. 12a. The surface exposed to dry air is located at position $x = 0$. The FSP is indicated by the horizontal dashed line. Initially, the wood was fully saturated by immersing the specimens in distilled water for at least one month, resulting in a homogeneous initial moisture distribution at about 160% MC. In Fig. 12a, the time between each profile, Δt, is 7 h and the duration of the drying period, t, is 6 days. The profiles were obtained by time interpolation and smoothening over space and time using profiles measured every 103 min. After a fast initial decrease in the MC to 140%, an evaporation front develops inside the sample. The fast initial decrease in MC throughout the sample can be explained by the existence of continuous liquid paths throughout the wood sample (Wiberg et al. 2000). When the continuity of the liquid phase is disrupted, liquid flow caused by capillary pressure is no longer possible. After this point, the moisture transport becomes internally limited, which results in the formation of an evaporation front.

Figure 12b shows the relaxation analysis, which is performed at three different points, similar to the water uptake analysis. At each position, the loss of bound water only starts just after all free water has vanished.

Moisture content profiles of oak and teak during drying are given in Fig. 13a and c. For oak, the profile
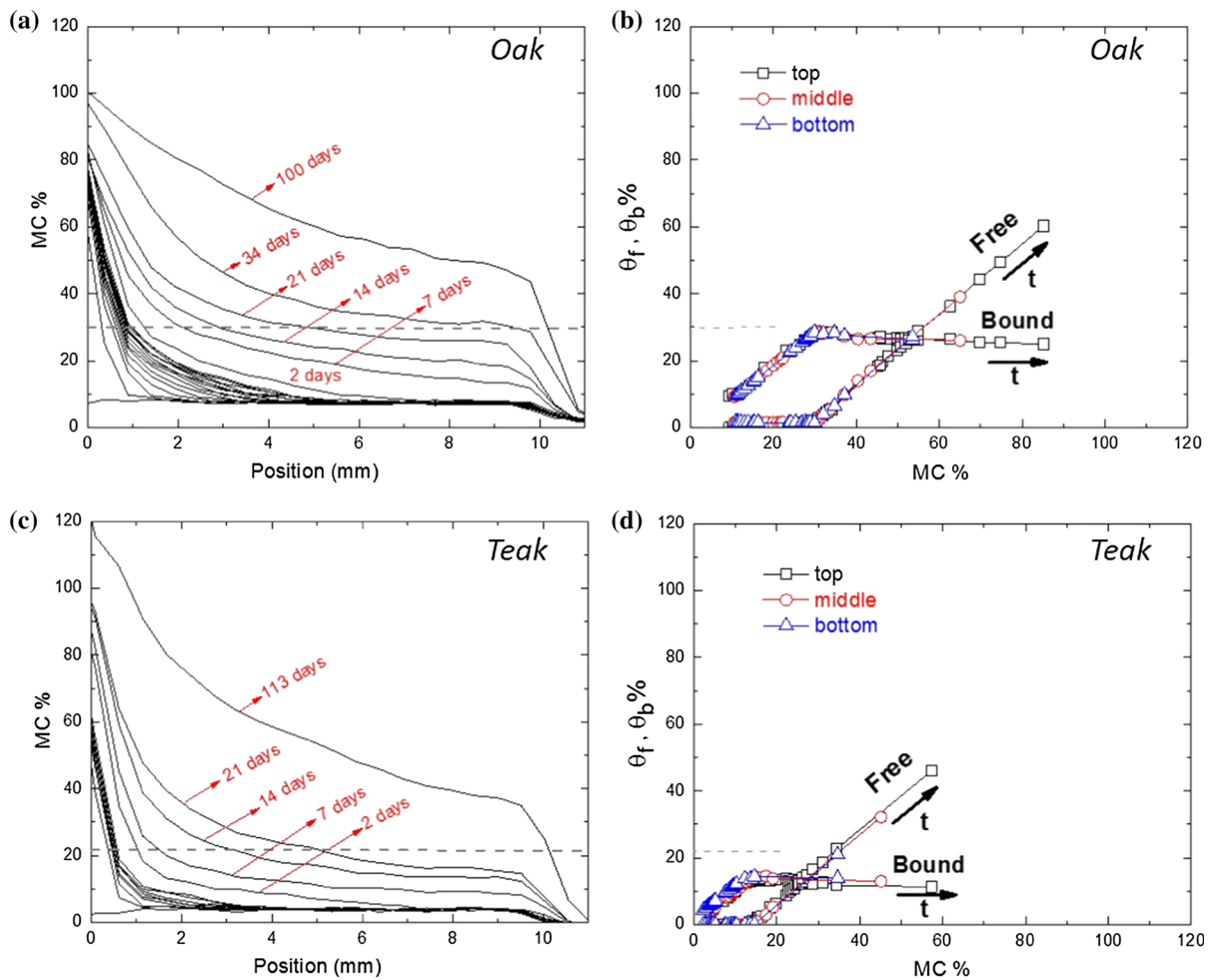
Fig. 11 The MC profiles during water uptake of **a** oak, and **c** teak. The profiles are given every 2 h for the first day and at the indicated times. Moisture fraction of free water, θ_f, and bound water, θ_b, versus total MC for **b** oak, and **d** teak, at 3 positions: around 2 mm (*top*), 5 mm (*middle*) and 8 mm (*bottom*) below the surface

prior to drying is flat with a 120% MC. A quick initial decrease in the MC to 100% is observed that could be the result of evaporation of liquid water present in ray tracheids. Additionally, more uniform drying rather than a sharp evaporation front is observed. This could be explained by the fast internal redistribution of liquid water via the longitudinal tracheids and wood rays (Wiberg et al. 2000). For teak, the profile prior to drying is flat with a 110% MC. Note that the time scale between two subsequent profiles is about three times more than that of pine sapwood and oak. Compared to the drying of pine sapwood and oak, the most visible difference is the absence of fast initial decrease in the MC. Immediately, a sharp evaporation front develops indicating internally limited transport.

The relaxation analyses at three different points are shown in Fig. 13b and d for oak and teak. Similar to pine sapwood, at each position, the loss of bound water starts just after vanishing the free water.

The curves show that in uptake and drying, always the same sequence of filling/emptying is followed. Obviously, there is a unique coupling between the MC and the fractions of bound and free water.

Effective diffusion coefficient

To answer the question how water migrates through wood, we study the effective diffusion coefficient, D_{eff}, found from the uptake and drying experiments. Firstly, the derivation of D_{eff} will be explained.
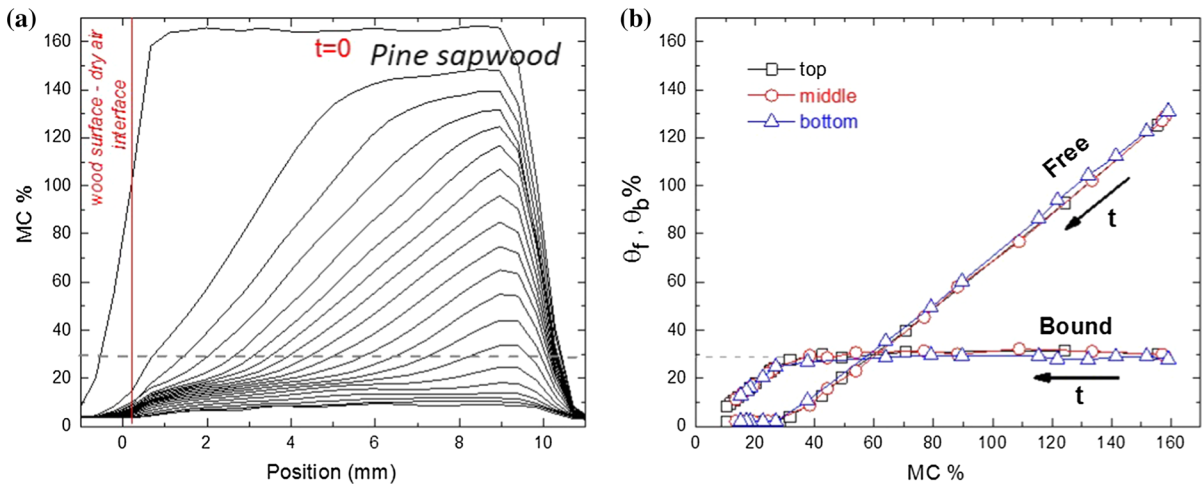
Fig. 12 a The MC profiles of pine sapwood during drying; $\Delta t = 7$ h, t = 6 days. **b** Moisture fraction of free water, θ_f, and bound water, θ_b, versus total MC at 3 positions similar to water

uptake, i.e. around 2 mm (*top*), 5 mm (*middle*) and 8 mm (*bottom*) below the surface

Secondly, the D_{eff} values will be calculated. Thirdly, the D_{eff} values will be interpreted to understand the dominant transport mechanism. Additionally, D_{eff} of the water uptake and drying will be compared.

Theory

The effective diffusivity can be determined directly from moisture profiles. One-dimensional moisture transport can be described by a non-linear equation (Bear and Bachmat 1990):

$$\frac{\partial \theta}{\partial t} = \frac{\partial}{\partial z}\left(D_{eff}\frac{\partial \theta}{\partial z}\right), \tag{2}$$

where θ is the moisture content, z is the position, t is the time and D_{eff} is the effective diffusivity. When the well-known Boltzmann transformation (Matano 1933) is applied:

$$\lambda = \frac{z}{\sqrt{t}} \tag{3}$$

the non-linear diffusion equation reduces to a differential equation:

$$2\frac{d}{d\lambda}\left(D_{eff}\frac{d\theta}{d\lambda}\right) + \lambda\frac{d\theta}{d\lambda} = 0, \tag{4}$$

In our case Eq. 4 has the following initial and boundary conditions:

$$\theta = \theta_\infty \text{ for } \lambda \to \infty (z > 0, t = 0) \tag{5}$$

$$\theta = \theta_0 \text{ for } \lambda = 0 (z = 0, t > 0) \tag{6}$$

where θ_∞ is the initial uniform moisture content of the sample and θ_0 is the boundary moisture content. $\theta_0 > \theta_\infty$ for water uptake, while $\theta_0 = 0$ for drying.

If D_{eff} is constant, Eq. 4 has an analytical solution for the water uptake process given by:

$$\theta = \theta_0 - (\theta_0 - \theta_\infty)erf\left(\frac{\lambda}{\xi}\right) \tag{7}$$

where ξ is defined as $\xi \equiv \sqrt{4D_{eff}}$.

In case of drying, $\theta_0 = 0$ in Eq. 7, which leads to:

$$\theta = \theta_\infty erf\left(\frac{\lambda}{\xi}\right). \tag{8}$$

Note that for small $\frac{\lambda}{\xi}$, $erf\left(\frac{\lambda}{\xi}\right)$ can be approximated by $\frac{2\lambda}{\sqrt{\pi}\xi}$. As such Eq. 8 can then be rewritten as:

$$\xi = \frac{2\lambda}{\sqrt{\pi}}\frac{\theta_\infty}{\theta}, \tag{9}$$

$$D_{eff} = \frac{\theta_\infty^2}{\pi}\left(\frac{\lambda}{\theta}\right)^2, \tag{10}$$

Experimental results

The Boltzmann transformation is applied for the moisture profiles for both uptake and drying experiments (until the front reaches the bottom, Figs. 10, 11,
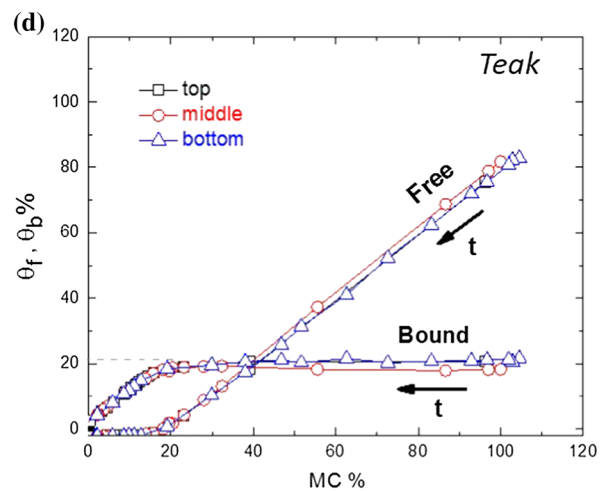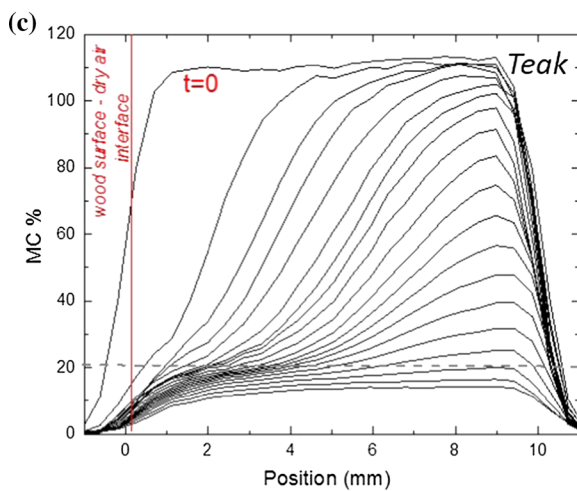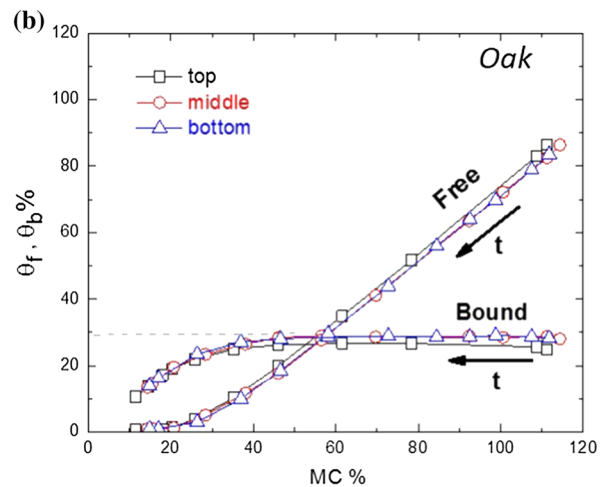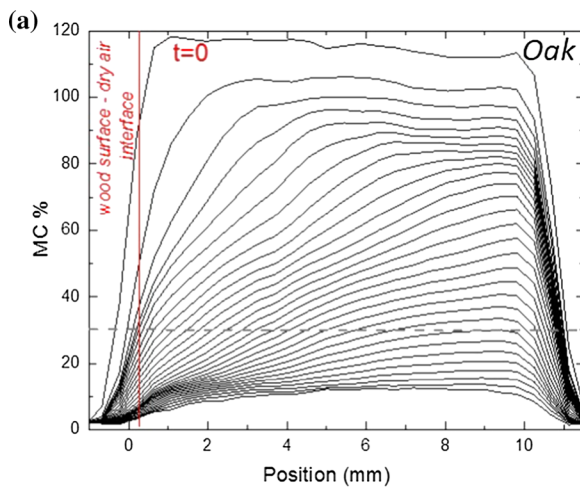
Fig. 13 The MC profiles during drying of **a** oak; Δt = 6.8 h, t = 8.5 days, **c** teak; Δt = 22.4 h, t = 18 days. Moisture fraction of free water, θf, and bound water, θb, versus total

MC for **b** oak, and **d** teak, at 3 positions: around 2 mm (*top*), 5 mm (*middle*) and 8 mm (*bottom*) below the surface

12, 13) and shown in Fig. 14. All the transformed profiles nicely overlap, except for the profiles of the oak drying experiment).

The effective diffusion coefficients (D_{eff}) for the water uptake experiments are determined by fitting the transformed profiles with Eq. 7. For drying Eq. 10 is used. We take for λ and θ the values λ* and θ* at the moisture content at the FSP, which is shown in the insets on the right column of Fig. 14. The diffusivity values are given in Table 3.

Table 3 shows that drying is faster than the water uptake for all the studied wood types, which is about 8 times faster for pine sapwood, about 1.5 times for oak, and about 5 times for teak.

Fig. 14 The profiles of the uptake and the drying after ▶ Boltzmann transformation. The graphs on the *left column* represents the water uptake, where the solid lines are the fitted error function, Eq. 7, from which D_{eff} is obtained. The graphs on *right column* represents drying, where the linear approximation below FSP is given in the inset figures and D_{eff} is obtained by Eq. 10

Interpreting the effective diffusivity

In order to have conceptual understanding of the transport mechanism, we evaluated two extreme diffusion models in terms of transport, and compared our experimental findings with the models. The models are assuming a good transport connectivity,
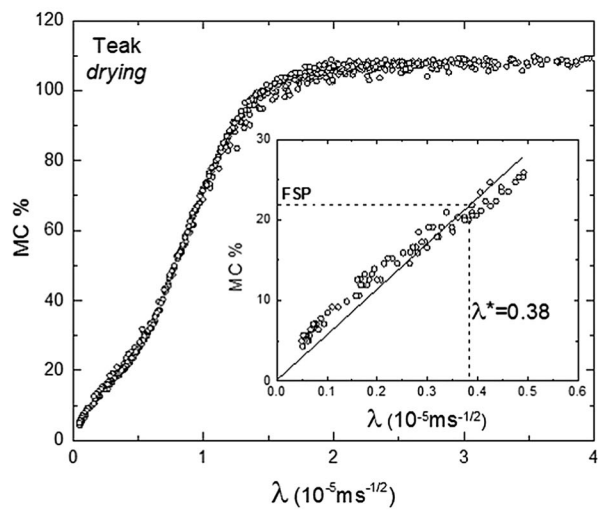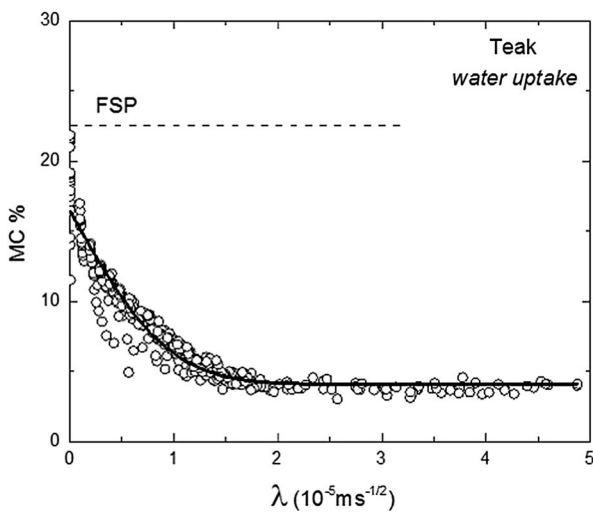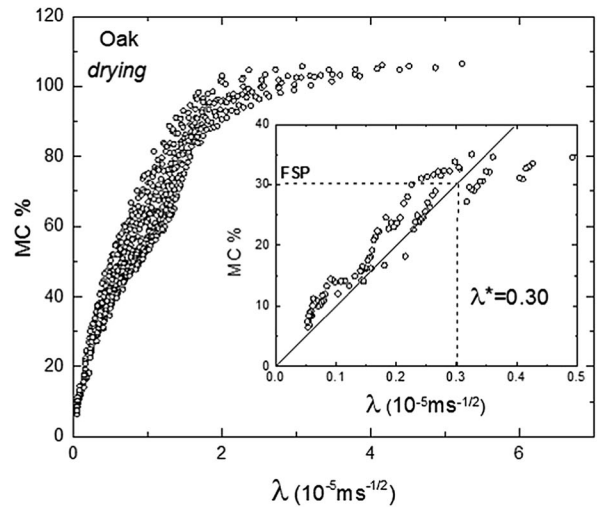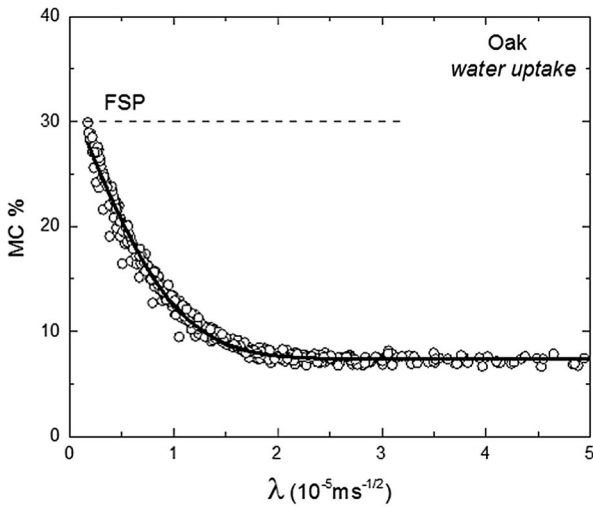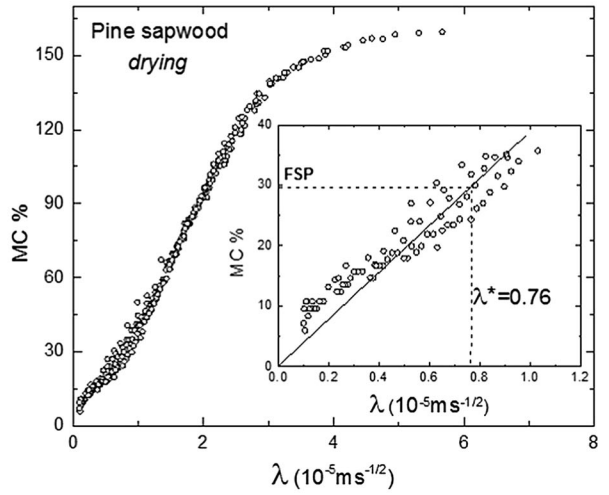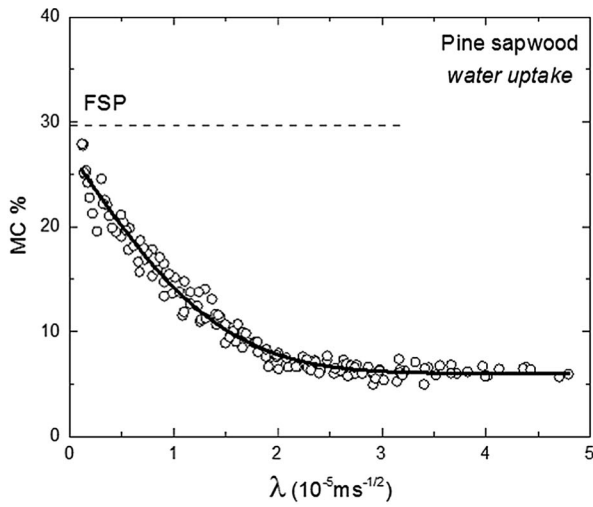
Table 3 D_{eff} values for pine sapwood, oak and teak for water uptake and drying as found from the Boltzmann transformed profiles

	D_{eff} (10^{-10} m²/s)	
	Water uptake	Drying
Pine sapwood	0.68	5.2
Oak	0.26	0.35
Teak	0.25	1.2

Table 4 Estimated theoretical diffusivity values for two diffusion models

	D_{eff} (10^{-10} m²/s)	
	Parallel	Series
Pine sapwood	8.5–34	0.25–2.0
Oak	4.0–23	0.17–1.4
Teak	8.6–2.8	0.13–2.8

Parallel diffusion in vapor phase and in the fibers

Series diffusion in vapor phase and in the fibers

Fig. 15 Schematic presentation of the considered diffusion concepts for wood. The *striped regions* represent the cell wall fibers, while the *blank regions* represents the lumen or other void spaces

and a poor connectivity, respectively. The derivation of these models is given in Appendix, and the basics of their foundation will be principally explained in the next subsection. A schematic presentation of both concepts is given in Fig. 15.

Model 1: parallel diffusion in vapor phase and in the fibers

In this case, it is assumed that the water vapor concentration in the lumen is in equilibrium with the cell wall moisture content (bound). The effective diffusion coefficient of the parallel model is estimated according to:

$$D_{eff}(\text{parallel}) \approx D_v \left(\frac{\partial c_v}{\partial c_b} \right), \tag{11}$$

where D_v is the water vapor diffusion coefficient. The change in the molar density of water vapor in lumen, c_v, with respect to the change in the molar density of bound water, c_b, is expressed by the inverse slope of the sorption isotherms in Fig. 6. Note that $D_v = D_{v,air}/\tau$, where τ is the tortuosity of wood for vapor. However, the tortuosity effect is not included in the calculation, since we aim to get an upper limit of D_{eff} by the parallel diffusion model. Additionally, as the lumen are rather straight, τ is not expected to exceed 2. The diffusivity values determined by Eq. 11 for 12% RH (MC of about 3.5%) and 100% RH (MC of about 22% for teak, 30% for pine sapwood and oak) are given in Table 4.

Model 2: series diffusion in vapor phase and in the fibers

The second model consists of series diffusion from wood cell to wood cell in vapor phase and in the fibers. The schematic representation of the model is given in Fig. 15. Two points have to be kept in mind; (1) the bound water in the cell wall has a much higher concentration than the water vapor in lumen, (2) the diffusion of water vapor in lumen is much faster than the diffusion in the cell wall. The effective diffusion coefficient of the series model is estimated according to:

$$D_{eff}(\text{series}) \approx \frac{D_b}{\varphi}, \tag{12}$$

where D_b is the bound-water diffusion coefficient and $\varphi \equiv L_b/L$. L_b is the length of the path for bound water, L_v is the length of the path for water vapor and L is the sum of them. φ is estimated based on the ratio of total moisture volume (in a fully saturated sample) per total volume of the sample. It is found as 0.16 for pine sapwood, 0.23 for oak and 0.31 for teak. The bound-

water diffusion coefficient is taken from literature that it is aimed to get a lower limit of D_{eff} by the series diffusion model. There is hardly information available, so the bound water diffusion coefficient for *Picea sitchensis* is used, which is 0.4×10^{-11} m^2/s at MC of 8% and 3.2×10^{-11} m^2/s at MC of 28% (Siau 1984). This diffusion coefficient is obtained by filling the lumens with a low-melting alloy of bismuth, lead, and tin. Considering these values, the diffusivity values calculated with Eq. 12 are given in Table 4.

The order of magnitude of theoretically derived diffusivity values from series model (Table 4) is closest to the order of magnitude of experimental results (Table 3) of both water uptake and drying. Therefore, the transport during water uptake and drying is better represented by the series model indicating that the diffusion in the cell wall fibers plays an important role.

Conclusions

It has been shown that NMR Imaging is a powerful method to determine the distribution and the concentration of water in wood, especially for understanding the water transport properties. A straightforward relation is obtained between the NMR signal and the moisture content. In contrast to weighing techniques, NMR relaxation analysis allows to identify the state of water within the wood, and to determine its order during wetting or emptied during drying. Based on this study, the following conclusions can be drawn, based on the studied wood types with the selected cut directions, regarding the water state and transport properties in pine sapwood, oak and teak during water uptake and drying:

1. The transport in all studied wood types is internally limited for both water uptake and drying. Internally limited means that the water movement is limited by water transport within the wood.
2. During water uptake, free water is observed only after the cell walls are filled with bound water at FSP. During drying of the water saturated samples, the loss of bound water starts just after free water is vanished, which has a transition point at FSP. Therefore, there is always local thermodynamic equilibrium of bound and free water during uptake and drying, i.e. the ratio between each state can always be found at any period.
3. The drying below FSP is faster than the water uptake for all studied wood types.
4. The transport during water uptake and drying is better represented by the conceptual model consisting of series diffusion from wood cell to wood cell in vapor phase and in the fibers. This indicates that the diffusion in the cell wall fibers plays an important role during both water uptake and drying.

Appendix

Observations with NMR are done in terms of moisture contents. Via uptake processes, an estimate of the diffusion coefficient is obtained. The appendix describes its interpretation.

Starting point is the non-linear diffusion equation:

$$\frac{\partial \theta}{\partial t} = \frac{\partial}{\partial z} D_{eff}(\theta) \frac{\partial \theta}{\partial z}, \tag{13}$$

where θ is the moisture content, z is the position, t is the time and D_{eff} is the effective diffusion constant. It can be written also in term of molar densities, c:

$$\frac{\partial c}{\partial t} = \frac{\partial}{\partial z} D_{eff}(c) \frac{\partial c}{\partial z}. \tag{14}$$

The question is how to come to a conceptual understanding of the effective diffusion coefficient. As water is either in the vapor phase (v) or in the fibers (bound, b):

$$c = c_v + c_b. \tag{15}$$

Model 1: parallel diffusion in vapor phase and in the fibers

Differential equation for water vapor in lumen:

$$\frac{\partial c_v}{\partial t} = \frac{\partial}{\partial z} D_v \frac{\partial c_v}{\partial z} - i, \tag{16}$$

Differential equation for bound water in the fibers:

$$\frac{\partial c_b}{\partial t} = \frac{\partial}{\partial z} D_b(c_b) \frac{\partial c_b}{\partial z} + i, \tag{17}$$

where i is the rate of change between vapor and bound state, D_b is the bound-water diffusion coefficient, and D_v is the water vapor diffusion coefficient. Summation of Eqs. 16 and 17 result in:

$$\frac{\partial c}{\partial t} = \frac{\partial}{\partial z} \left(\frac{D_v}{1 + \partial c_b/\partial c_v} + \frac{D_b}{1 + \partial c_v/\partial c_b} \right) \frac{\partial c}{\partial z}, \tag{18}$$

To arrive at Eq. 14, we take the effective diffusion coefficient as:

$$D_{eff} = \frac{D_v}{1 + \partial c_b/\partial c_v} + \frac{D_b}{1 + \partial c_v/\partial c_b}. \tag{19}$$

In case of water in wood: $c_v \ll c_b$ and therefore $\partial c_v/\partial c_b \ll 1$ (the water vapor density is low). As a consequence:

$$D_{eff} \approx D_v \frac{\partial c_v}{\partial c_b} + D_b \tag{20}$$

As diffusion in the fibers is much smaller compared to vapor diffusion, further simplification is possible:

$$D_{eff} \approx D_v \left(\frac{\partial c_v}{\partial c_b} \right). \tag{21}$$

Note that $D_v = D_{v,air}/\tau$ where τ is the tortuosity of wood for vapor, considered to be 2 at most. $D_{v,air} = 2.4 \times 10^{-5} \text{m}^2/\text{s}$ at 20 °C.

Model 2: series diffusion in vapor phase and in the fibers

In case of diffusion from wood cell to wood cell, chained in series, we can write the local molar fluxes for bound water in the cell wall fibers and vapor in the lumen as:

Locally the molar fluxes obey:

$$J_b = -D_b \frac{\partial c_b}{\partial z} = -D_b \left(\frac{\partial c_b}{\partial c_v} \right) \frac{\partial c_v}{\partial z}, \tag{22}$$

$$J_v = -D_v \frac{\partial c_v}{\partial z} \tag{23}$$

In a steady-state situation and in case of small gradients, the total flux being the sum of Eqs. 22 and 23, can be written as:

$$J \equiv -D_{eff} \frac{\Delta c}{L} = -D_{eff} \left(1 + \frac{\partial c_b}{\partial c_v} \right) \frac{\Delta c_v}{L}. \tag{24}$$

Further it can be derived that:

$$\Delta c_v = -J \left[\frac{L_b}{D_b \partial c_b/\partial c_v} + \frac{L_v}{D_v} \right], \tag{25}$$

where L_b is the length of the path for bound water, L_v is the length of the path for water vapor and L is the sum. In case we define $\varphi \equiv L_b/L$, the combination leads to:

$$D_{eff} \left(1 + \frac{\partial c_b}{\partial c_v} \right) = \frac{1}{\varphi/D_b(\partial c_b/\partial c_v) + (1-\varphi)/D_v} \tag{26}$$

As diffusion in the fibers is much smaller compared to vapor diffusion, $D_b \ll D_v$, and in case of low vapor density, $c_v \ll c_b$:

$$D_{eff} = \frac{D_b}{\varphi} \tag{27}$$

References

Almeida G, Gagné S, Hernández RE (2007) A NMR study of water distribution in hardwoods at several equilibrium moisture contents. Wood Sci Technol 41:293–307. doi:10.1007/s00226-006-0116-3

Araujo CD, MacKay AL, Hailey JRT, Whittall KP, Le H (1992) Proton magnetic resonance techniques for characterization of water in wood: application to white spruce. Wood Sci Technol 26:101–113. doi:10.1007/BF00194466

Araujo CD, Mackay AL, Whittall KP, Hailey JRT (1993) A diffusion model for spin-spin relaxation of compartmentalized water in wood. J Magn Reson Ser B 101(3):248–261. doi:10.1006/jmrb.1993.1041

Bear J, Bachmat Y (1990) Introduction to modeling of transport phenomena in porous media, vol 1. Springer, Berlin

Bucur V (2003) Nondestructive characterization and imaging of wood. Springer, Berlin Heidelberg

Bulian F, Jon G (2009) Wood coatings: theory and practice. Elsevier Science, New York

Carr HY, Purcell EM (1954) Effects of diffusion on free precession in nuclear magnetic resonance experiments. Phys Rev 94(3):630–638. doi:10.1103/PhysRev.94.630

Casieri C, Senni L, Romagnoli M, Santamaria U, De Luca F (2004) Determination of moisture fraction in wood by mobile NMR device. J Magn Reson 171:364–372. doi:10.1016/j.jmr.2004.09.014

Donkers PAJ, Huinink HP, Erich SJF, Reuvers NJW, Adan OCG (2013) Water permeability of pigmented waterborne coatings. Prog Org Coat 76(1):60–69. doi:10.1016/j.porgcoat.2012.08.011

Dvinskikh SV, Furó I, Sandberg D, Söderström O (2011a) Moisture content profiles and uptake kinetics in wood cladding materials evaluated by a portable nuclear magnetic resonance spectrometer. Wood Mat Sci Eng 6:119–127. doi:10.1080/17480272.2010.543288 (April 2013)

Dvinskikh SV, Henriksson M, Mendicino AL, Fortino S, Toratti T (2011b) NMR Imaging study and multi-fickian numerical simulation of moisture transfer in Norway spruce samples. Eng Struct 33(11):3079–3086. doi:10.1016/j.engstruct.2011.04.011

Gezici-Koç Ö, Thomas CAAM, Michel M-EB, Erich SJF, Huinink HP, Flapper J, Duivenvoorde FL, van der Ven LGJ, Adan OCG (2016) In-depth study of drying solvent-borne alkyd coatings in presence of Mn- and Fe- based catalysts as cobalt alternatives. Mater Today Commun 7(June):22–31. doi:10.1016/j.mtcomm.2016.03.001

Hahn EL (1950) Spin echoes. Phys Rev 80(4):580–594. doi:10.1103/PhysRev.80.580

Hameury S, Sterley M (2006) Magnetic resonance imaging of moisture distribution in *Pinus Sylvestris L.* exposed to daily indoor relative humidity fluctuations. Wood Mater Sci Eng 1(December 2013):116–126. doi:10.1080/17480270601150578

Kekkonen PM, Ylisassi A, Telkki VV (2014) Absorption of water in thermally modified pine wood as studied by nuclear magnetic resonance. JOUR. J Phys Chem C 118(4):2146–2153. doi:10.1021/jp411199r

Labbé N, De Jéso B, Lartigue J-C, Daudé G, Pétraud M, Ratier M (2002) Moisture content and extractive materials in maritime pine wood by low field 1H NMR. Holzforschung. doi:10.1515/HF.2002.005

Matano C (1933) On the relation between the diffusion coefficients and the concentrations of solid metals (the nickel-copper system). Jpn J Phys 8:109–113

Menon RS, MacKay AL, Hailey JRT, Bloom M, Burgess AE, Swanson JS (1987) An NMR determination of the physiological water distribution in wood during drying. J Appl Polym Sci 33:1141–1155. doi:10.1002/app.1987.070330408

Passarini L, Malveau C, Hernández RE (2014) Water state study of wood structure of four hardwoods below fiber saturation point with nuclear magnetic resonance. Wood Fiber Sci 46(4):480–484

Peemoeller H, Weglarz WP, Jason Hinek M, Holly R, Lemaire C, Teymoori R, Liang J, Crone J, Mansour FK, Hartley ID (2013) NMR detection of liquid-like wood polymer component in dry aspen wood. Polymer 54(5):1524–1529. doi:10.1016/j.polymer.2012.12.081

Quick JJ, Hailey JRT, MacKay AL (2007) Radial moisture profiles of cedar sapwood during drying: a proton magnetic resonance study. Wood Fiber Sci 22(4):404–412

Riggin MT, Sharp AR, Kaiser R, Schneider MH (1979) Transverse NMR relaxation of water in wood. J Appl Polym Sci. doi:10.1002/app.1979.070231101

Robertson MB, Packer KJ (1999) Diffusion of D₂O in archaeological wood measured by 1-D NMR profiles. Appl Magn Reson 17:49–64. doi:10.1007/BF03162068

Rosenkilde A, Glover P (2002) High resolution measurement of the surface layer moisture content during drying of wood using a novel magnetic resonance imaging technique. Holzforschung 56:312–317. doi:10.1515/HF.2002.050

Sandberg K, Salin J-G (2010) Liquid water absorption in dried Norway spruce timber measured with CT scanning and viewed as a percolation process. Wood Sci Technol 46(1–3):207–219. doi:10.1007/s00226-010-0371-1

Sedighi-Gilani M, Griffa M, Mannes D, Lehmann E, Carmeliet J, Derome D (2012) Visualization and quantification of liquid water transport in softwood by means of neutron radiography. Int J Heat Mass Transf 55(21–22):6211–6221. doi:10.1016/j.ijheatmasstransfer.2012.06.045

Siau JF (1984) Transport processes in wood. In: Timell TE (ed) Springer series in wood science, vol 2. Springer, Berlin. doi:10.1007/978-3-642-69213-0

Skaar C (1988) Wood-water relations. In: Springer series in wood science. Springer, Berlin. doi:10.1007/978-3-642-73683-4

Stamm AJ (1971) Review of nine methods for determining the fiber saturation points of wood and wood products. Wood Sci 4(2):114–128

Stenström S, Catherine B, Foucat L (2014) Magnetic resonance imaging for determination of moisture profiles and drying curves. In: Tsotsas E, Mujumdar AS (eds) Modern drying technology, set. Wiley-VCH Verlag GmbH & Co. KGaA, Weinheim, Germany. doi:10.1002/9783527631728.ch10

Telkki VV, Yliniemi M, Jokisaari J (2013) Moisture in softwoods: fiber saturation point, hydroxyl site content, and the amount of micropores as determined from NMR relaxation time distributions. Holzforschung 67(3):291–300. doi:10.1515/hf-2012-0057

Thygesen LG, Elder T (2009) Moisture in untreated, acetylated, and furfurylated Norway spruce monitored during drying below fiber saturation using time Domain NMR. Wood Fiber Sci 41(2):194–200

Topgaard D, Söderman O (2002) Changes of cellulose fiber wall structure during drying investigated using NMR self-diffusion and relaxation experiments. Cellulose 9(2):139–147. doi:10.1023/A:1020158524621

Van Meel PA, Erich SJF, Huinink HP, Kopinga K, De Jong J, Adan OCG (2011) Moisture transport in coated wood. Prog Org Coat 72(4):686–694. doi:10.1016/j.porgcoat.2011.07.011

Wiberg P, Sehlstedt-P SMB, Morén TJ (2000) Heat and mass transfer during sapwood drying above the fibre saturation point. Dry Technol 18(8):1647–1664. doi:10.1080/07373930008917804

Zhang MH, Wang XM, Gazo R (2013) Water states in yellow poplar during drying studied by time-domain nuclear magnetic resonance. Wood Fiber Sci 45(4):423–428